Available online at www.sciencedirect.com
SCIENCE DIRECT®
Journal of Contaminant Hydrology 73 (2004) 145–179
JOURNAL OF Contaminant Hydrology
www.elsevier.com/locate/jconhyd

A triple-continuum approach for modeling flow and transport processes in fractured rock

Yu-Shu Wu*, H.H. Liu, G.S. Bodvarsson

Earth Sciences Division, Lawrence Berkeley National Laboratory, 1 Cyclotron Road, MS 90-1116, Berkeley, CA 94720, USA

Received 4 September 2003; received in revised form 16 December 2003; accepted 9 January 2004

Abstract

This paper presents a triple-continuum conceptual model for simulating flow and transport processes in fractured rock. Field data collected from the unsaturated zone of Yucca Mountain, a repository site of high-level nuclear waste, show a large number of small-scale fractures. The effect of these small fractures has not been considered in previous modeling investigations within the context of a continuum approach. A new triple-continuum model (consisting of matrix, small-fracture, and large-fracture continua) has been developed to investigate the effect of these small fractures. This paper derives the model formulation and discusses the basic triple-continuum behavior of flow and transport processes under different conditions, using both analytical solutions and numerical approaches. The simulation results from the site-scale model of the unsaturated zone of Yucca Mountain indicate that these small fractures may have an important effect on radionuclide transport within the mountain.

Keywords: Naturally fractured reservoir; Dual-continuum porous media; Double-porosity; Dual-permeability; Triple-continuum model; Numerical reservoir simulation; Fractured unsaturated rock

1. Introduction

The study of flow and transport processes in fractured rock has recently received increased attention because of its importance to underground natural-resource recovery, waste storage, and environmental remediation. Since the 1960s, significant progress has been made towards the understanding and modeling of flow and transport processes in fractured rock (Barenblatt et al., 1960; Warren and Root, 1963; Kazemi, 1969; Kazemi et

* Corresponding author. Tel.: +1-510-486-7291; fax: +1-510-486-5686.
E-mail address: YSWu@lbl.gov (Y.-S. Wu).

0169-7722/$ - see front matter
doi:10.1016/j.jconhyd.2004.01.002

al., 1992; Pruess and Narasimhan, 1985). Despite these advances, modeling the coupled processes of multiphase fluid flow, heat transfer, and chemical migration in a fractured porous medium remains a conceptual and mathematical challenge. The challenge arises primarily from (1) the inherent heterogeneity and uncertainties associated with the characterization of a fracture–matrix system for any field-scale problem, and (2) the difficulties in conceptualizing, understanding, and describing flow and transport processes in such a system.

Mathematical modeling using a continuum approach involves developing conceptual models, incorporating the geometrical information of a given fracture–matrix system, and setting up the general mass and energy conservation equations for overlapping fracture–matrix domains. The majority of the computational effort is used to solve the governing equations that couple fluid and heat flow with chemical migration either analytically or numerically. The key issue for simulating flow and transport in fractured rock is how to handle fracture–matrix interactions under different conditions involving multiple processes. The commonly used mathematical methods for dealing with such interactions include: (1) an explicit discrete-fracture and matrix model (e.g., Snow, 1965; Sudicky and McLaren, 1992), (2) the dual-continuum method [including double- and multi-porosity, dual-permeability, or the more general "multiple interacting continua" (MINC) method (e.g., Barenblatt et al., 1960; Warren and Root, 1963; Kazemi, 1969; Pruess and Narasimhan, 1985; Wu and Pruess, 1988)], and (3) the effective-continuum method (ECM) (e.g., Wu, 2000).

The explicit discrete-fracture approach is, in principle, a more rigorous model than a continuum one, and the application of this method may be computationally intensive. Furthermore, it requires a detailed knowledge of fracture and matrix geometric properties and their associated spatial distributions (which are rarely known at a given site). This approach becomes more difficult and demanding when modeling multiphase flow and thermal processes in a complicated fracture–matrix system, which requires detailed spatial discretization of both fracture and matrix systems. For these reasons, this approach has up to now found only limited field application in modeling multiphase, nonisothermal flow and transport processes in fractured rocks.

The dual-continuum method, on the other hand, is conceptually appealing and computationally less demanding than the discrete-fracture approach. It is able to handle fracture–matrix interactions more easily than the discrete-fracture model; thus it has commonly been used for modeling fluid flow, heat transfer, and chemical transport through fractured reservoirs. One type of dual-continuum method, the classical double-porosity model, was developed in the early 1960s (Barenblatt et al., 1960; Warren and Root, 1963). In this model, a flow domain is composed of matrix blocks with low permeability, embedded in a network of interconnected fractures, with global flow and transport in the formation occurring only through the fracture system conceptualized as an effective continuum. The model treats matrix blocks as spatially distributed sinks or sources to the fracture system and fracture–matrix interflow as a quasi-steady state (Warren and Root, 1963).

In an attempt to incorporate additional matrix–matrix interactions, the dual-permeability model has been developed and implemented into a numerical scheme of nonisothermal multiphase fluid and heat flow in fractured rock (Pruess, 1991). This type of dual-continuum model considers global flow occurring not only between fractures but also between matrix gridblocks. In this approach, the fractures and the matrix are each

represented by separate gridblocks that are connected to each other. The same quasi-steady state flow assumption as that in the double-porosity concept (Warren and Root, 1963) is used to handle fracture–matrix interflow.

As a generalization of the dual-continuum model, the more rigorous MINC concept (Pruess and Narasimhan, 1985) describes gradients of pressures, temperatures, and concentrations between fractures and matrix by further subdividing individual matrix blocks. This approach provides a better approximation for transient fracture–matrix interactions than the quasi-steady state flow assumption used in the double-porosity or dual-permeability model. Fluid and heat flow and transport between fracture and matrix blocks can be modeled by means of one- or multi-dimensional strings of nested gridblocks. However, it should be mentioned that the applicability of such dual-continuum approaches is in general dependent upon (1) relatively uniform distribution of fracture networks and (2) knowledge of fracture and matrix properties.

As an alternative method, the ECM represents fractures and rock matrix as a single effective continuum. The ECM has long been used for modeling fracture–matrix flow because of its simple data requirements and computational efficiency. This approach may be applicable to modeling multiphase, nonisothermal flow and solute transport in fractured porous media under near-thermodynamic-equilibrium conditions (Wu, 2000). When rapid flow and transport processes occur in subsurface fractured reservoirs, however, thermodynamic equilibrium conditions cannot (in general) hold.

Investigations concerning the feasibility of using the unsaturated zone (UZ) of Yucca Mountain as a repository for high-level nuclear waste have generated considerable research interest in understanding and modeling flow and transport processes in unsaturated fractured rock. Since the 1980s, a number of numerical models have been developed specifically for evaluating UZ hydrologic conditions at Yucca Mountain. Studies before the 1990s primarily used one- and two-dimensional models to understand basic flow and transport processes in fractured rock (Rulon et al., 1986; Pollock, 1986; Tsang and Pruess, 1987). In the early 1990s, Wittwer et al. (1995) began development of a three-dimensional (3-D) model using an ECM approach and incorporating many geological and hydrological complexities. Ahlers et al. (1995) continued this work by increasing the numerical and spatial resolution of the 3-D ECM UZ model. Their studies considered processes such as gas pressures and moisture flow, temperature and heat flow analyses, and rock-property evaluation through inverse modeling. Since then, more comprehensive mountain-scale numerical models (e.g., Wu et al., 1998, 1999, 2002) have been developed to study flow processes in the UZ of Yucca Mountain, using the more rigorous dual-permeability concept. A comparative study of the different approaches for handling fracture–matrix interactions was conducted as part of the effort to investigate rapid movement of solute in fractured tuffs at Yucca Mountain (McLaren et al., 2000).

Although many conceptual models for fracture–matrix interaction have been evaluated for Yucca Mountain site characterization studies (Doughty, 1999), the most widely used model has been the dual-permeability concept. It was chosen for use in site characterization in part because it has proved to be capable of matching many types of field-observed data (e.g., Wu et al., 1998, 1999). Another consideration is that net infiltration rates at the site are estimated to be very low (on the order of millimeters/year) or close to saturated

matrix hydraulic conductivity. In this case, global flow through the matrix can no longer be ignored. However, results from recent field studies and tests, in particular fracture mapping data (Liu et al., 2000) collected along the walls of the underground tunnels, reveal that there exists a significantly large variety in fracture sizes, from centimeters to tens of meters. Considerable numbers of small-scale fractures have not been considered in the previous modeling studies. Although the majority of these small fractures may not contribute much to global flow and transport through the UZ system, they may provide additional connection areas for interflow between well-connected, large-scale fractures and surrounding matrix blocks, which ultimately affects fracture–matrix interactions. In addition, they may offer a buffer zone for interaction between well-connected large fracture and the matrix, because of their high storage capacity compared to that of large fractures. On the other hand, the currently used dual-permeability model is unable to incorporate the effects of these small fractures.

The objectives of this study are (1) to propose a triple-continuum concept to study the effect of small-scale fractures on flow and transport processes in fractured rock; (2) to develop a methodology for determining model parameters of the proposed model; and (3) to demonstrate application of the proposed model to site characterization of the Yucca Mountain UZ. In particular, we investigate the triple-continuum behavior of flow and transport processes in fractured rocks using both numerical modeling results and an analytical solution (Liu et al., 2003). We discuss issues related to the determination of small-fracture properties using observations from single-phase flow and transport tests. As application examples, we demonstrate how to apply the proposed triple-continuum model to field problems at Yucca Mountain in (1) estimating model-related fracture–matrix parameters using field observed data and an inverse-modeling approach; and (2) simulating 3-D site-scale flow and transport.

2. Triple-continuum concept and mathematical formulation

Following the pioneering work by Barenblatt et al. (1960) and Warren and Root (1963), several triple-porosity models have been proposed in the literature (e.g., Closemann, 1975; Wu and Ge, 1983; Abdassah and Ershaghis, 1986; Bai et al., 1993) for describing flow through fractured rocks. Liu et al. (2003) has recently presented a new triple-porosity model for flow in a fracture–matrix system that includes cavities within the rock matrix (as an additional porous portion of the matrix) of the Yucca Mountain UZ formation. In general, these developed models have been focused on handling the heterogeneity of the rock matrix (i.e., subdividing the rock matrix into two or more subdomains with different porous medium properties).

During the last decade, a considerable amount of fracture data has been mapped at the Yucca Mountain site. Most fracture data sets obtained in these data collection efforts exclude small-scale fractures (with tracer lengths <0.5 m) (Liu et al., 2000). Actual observation of fractures along the underground tunnel walls reveals that many "small" fractures exist in the unsaturated tuffs of the site. Recently, more fracture mapping data have been collected from a small-scale detailed line survey (DLS) (US Geological Survey, unpublished report). Fig. 1 presents a plot of measured fracture-trace lengths versus frequency distribution, using

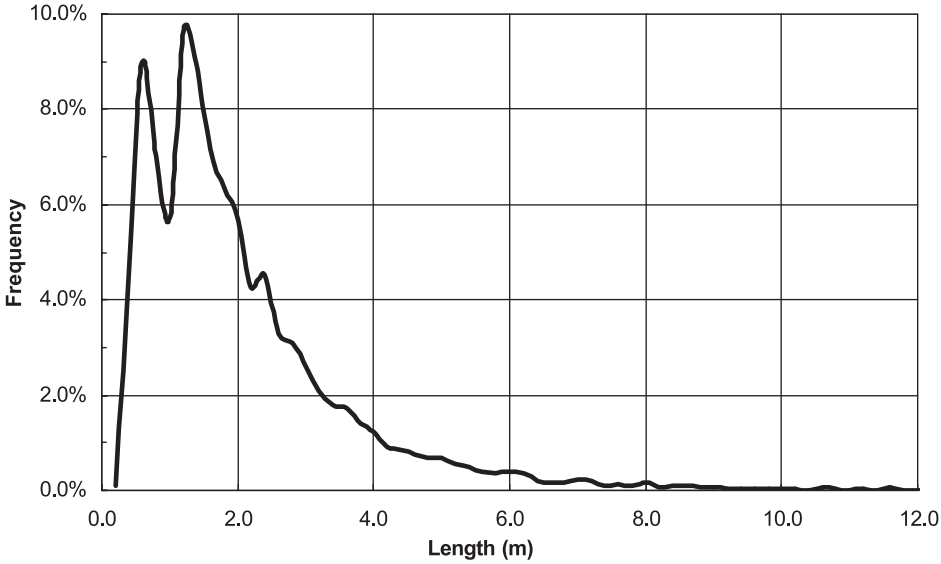

Fig. 1. Frequency distribution for trace lengths of mapped fractures from the Tptpmn unit.

statistics of 12,425 fractures, mapped from the Topopah Spring middle nonlithophysal unit (Tptpmn), a host layer for the potential repository. Fig. 2a shows a distribution realization for 2-D fracture networks of a vertical 20×20 m domain, with the randomly generated fracture network on the figure based on statistical distributions of fracture-trace lengths (>0.35 m), fracture density, and orientations (or dipping angles from the horizontal direction). Fig. 2b displays the actual flow paths along the fractures from the top to the bottom boundaries of the 2-D domain, created from a flow simulation by imposing different pressure heads on the two boundaries.

Field-observed fracture data, as well as their statistical analyses (Figs. 1 and 2), indicate a large number of small- to intermediate-scale fractures of trace length ~1.0 m in the Tptpmn unit (note that mapped fractures excluded an even greater number of smaller fractures of less than 0.2 m.) A recent numerical study of unsaturated flow in a fracture network (Liu et al., 2003a) including fractures shorter than 0.5 m shows that many small-scale fractures that are well connected only locally to fractures along global-flow paths do not directly contribute to global flow. These small-scale fractures significantly increase contact areas between fractures and matrix systems, which may potentially impact overall flow and transport processes.

To capture effects of small-scale fractures, we conceptualize the fracture–matrix system as consisting of a single porous-medium rock matrix and two types of fractures: (1) "large" *globally connected* fractures and (2) "small" fractures that are *locally connected* to the large fractures and the rock matrix. Fig. 3 illustrates the triple-continuum concept compared to ECM, double-porosity, and dual-permeability concepts. The triple-continuum method (Fig. 3d) extends the dual-permeability concept by adding one more connection (via small fractures) between the large fractures and the matrix blocks. Note that fractures not directly connected with large fractures (i.e., fractures that are isolated within the

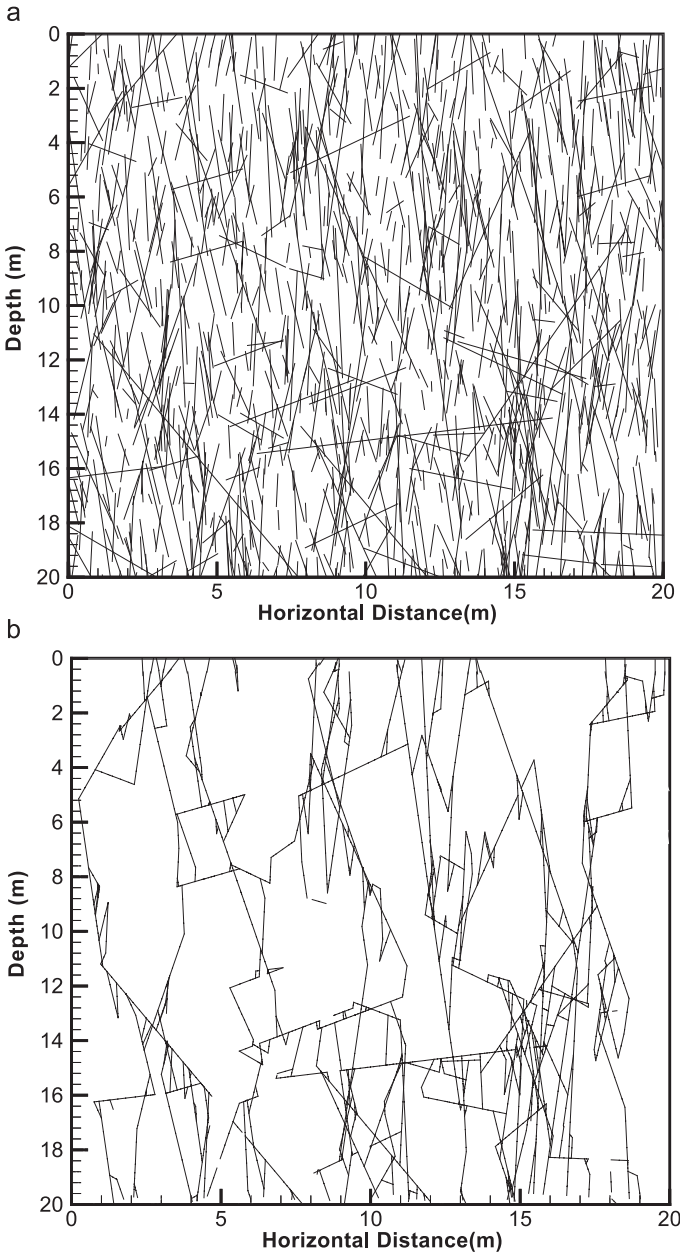

Fig. 2. (a) Generated vertical fracture network based on statistical distributions of fracture-trace lengths, density, and orientations of fracture data, observed at the Tptpmn unit. (b) Vertical fracture network: global flow paths along large fractures.

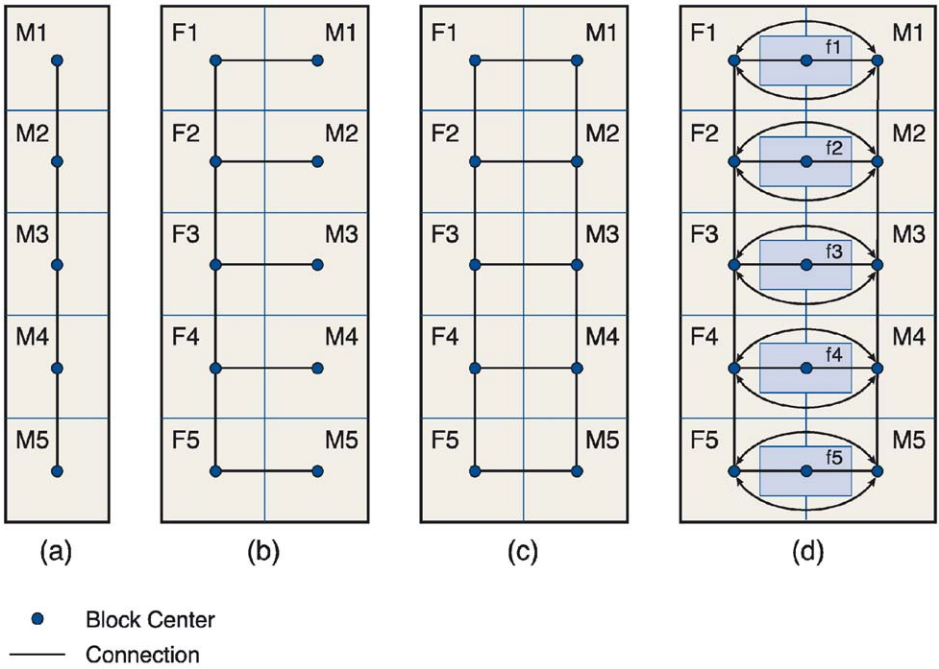

Fig. 3. Schematic of different conceptualizations for handling fracture–matrix interactions: (a) effective-continuum model (ECM); (b) double-porosity model; (c) dual-permeability model; and (d) triple-continuum model. (M=matrix; F=large fractures; f=small fractures).

matrix) are not considered part of the small fracture continuum in this model. Instead, these fractures are considered as part of the matrix continuum.

Fig. 4 illustrates the triple-continuum conceptualization for a fracture–matrix system in which the small-fracture/matrix connections occur in only one dimension (shown horizontally). A second set of small-fracture/matrix connections can also be added to occur in two dimensions (i.e., horizontally and vertically, Fig. 5). In a similar manner, a third set of fractures can be added to extend the system of small-fracture/matrix interactions to occur in three dimensions. Note that the triple-continuum model is not limited to the orthogonal idealization of the fracture systems illustrated in Figs. 4 and 5. Irregular and stochastic distributions of small and large fractures can be handled using a similar approach to the MINC methodology (Pruess, 1983), as long as the actual distribution patterns are known.

In principle, the proposed triple-continuum model, like the dual-continuum approach, uses an "effective" porous medium to approximate the two types of fractures and the rock matrix, and considers the three continua to be spatially overlapped. Like other continuum approaches, the triple-continuum model relies on the assumption that approximate thermodynamic equilibrium exists (locally) within each of the three continua at all times at a given location. Based on the local equilibrium assumption, we can define thermodynamic variables, such as pressures, concentrations, and temperatures, for each continuum.

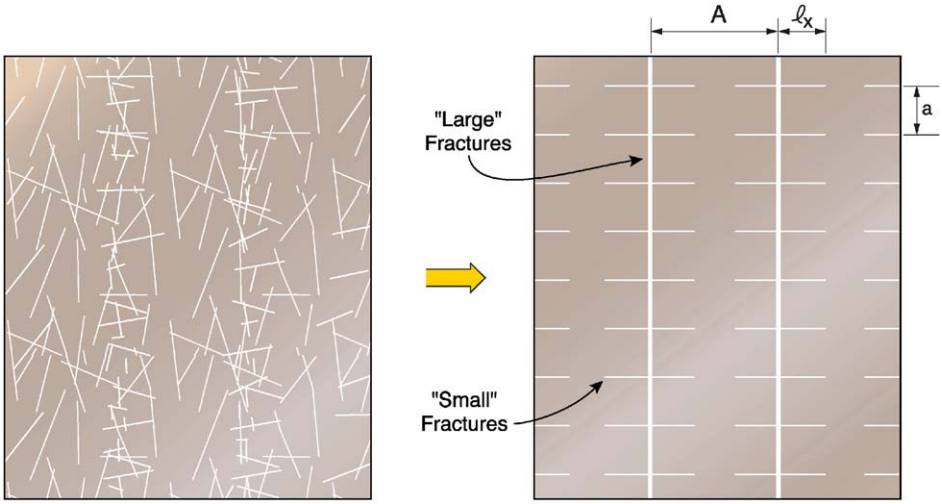

Fig. 4. Basic conceptualization for triple-continuum approximation of one-dimensional large-fracture, small-fracture, and rock matrix systems.

In the triple-continuum approach, processes of flow and transport in fractured rocks are described separately, using a triplet of governing equations for the two fracture and matrix continua. This conceptualization results in a set of partial differential equations for flow and transport in each continuum, which are in the same form as that for a single porous medium. Let us consider a two-phase (liquid and gas) nonisothermal system. The

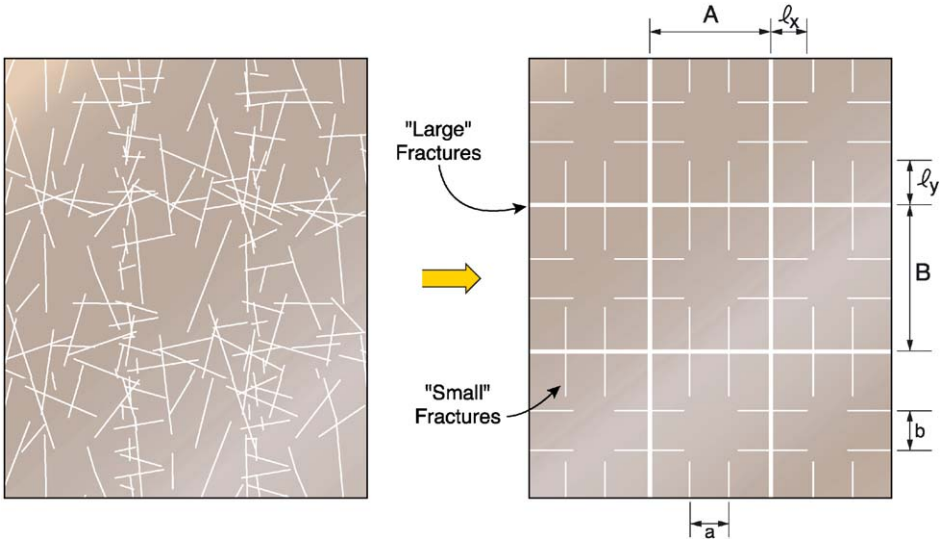

Fig. 5. Basic conceptualization for triple-continuum approximation of two-dimensional large-fracture, small-fracture, and rock matrix systems.

corresponding transport equation of each component κ in the two-phase system within each of three continua can be written as follows:

$$\frac{\partial}{\partial t}\left\{\phi\sum_{\beta}(\rho_{\beta}S_{\beta}X_{\beta}^{\kappa})+(1-\phi)\rho_{s}\rho_{L}X_{L}^{\kappa}K_{d}^{\kappa}\right\}$$
$$+\lambda_{\kappa}\left\{\phi\sum_{\beta}(\rho_{\beta}S_{\beta}X_{\beta}^{\kappa})+(1-\phi)\rho_{s}\rho_{L}X_{L}^{\kappa}K_{d}^{\kappa}\right\}$$
$$=-\sum_{\beta}\nabla\cdot(\rho_{\beta}X_{\beta}^{\kappa}\boldsymbol{v}_{\beta})+\sum_{\beta}\nabla\cdot(\rho_{\beta}\underline{D}_{\beta}^{\kappa}\cdot\nabla X_{\beta}^{\kappa})+q^{\kappa} \tag{1}$$

and the energy conservation equation is:

$$\frac{\partial}{\partial t}\left\{\sum_{\beta}(\phi\rho_{\beta}S_{\beta}U_{\beta})+(1-\phi)\rho_{s}U_{s}\right\}$$
$$=-\sum_{\beta}\nabla\cdot(h_{\beta}\rho_{\beta}\boldsymbol{v}_{\beta})+\sum_{\beta}\sum_{\kappa}\nabla\cdot(\rho_{\beta}h_{\beta}^{\kappa}\underline{D}_{\beta}^{\kappa}\cdot\nabla X_{\beta}^{\kappa})+\nabla\cdot(K_{th}\nabla T)+q^{E} \tag{2}$$

where subscript β is an index for fluid phase (β=L for liquid and g for gas), and κ is an index for components. (Other symbols and notations are defined in the table of nomenclature [included at the end of the text]). Note that chemical reaction terms in Eq. (1) can be more general than only retardation and first-order decay in the governing equations above. In general, Eqs. (1) and (2) can be used to describe flow and transport processes within each of the three continua. When applied, however, these equations are further simplified for small fracture and matrix continua, and their coupling is treated using physically based approaches, as discussed in Sections 3 (numerically) and 4 (analytically).

3. Numerical implementation

The numerical implementation of the triple-continuum model discussed above is based on the framework of the TOUGH2 code (Pruess, 1991; Wu and Pruess, 2000). The component mass- and energy-conservation equations (Eqs. (1) and (2), respectively) are discretized in space using an integral finite-difference method. The time discretization is carried out with a backward, first-order, finite-difference scheme. The discrete nonlinear equations for water, air, tracer/solute/radionuclide, and heat at a gridblock n can be written as follows:

$$R_{n}^{\kappa,k+1}=M_{n}^{\kappa,k+1}(1+\lambda_{k}\Delta t)-M_{n}^{\kappa,k}-\frac{\Delta t}{V_{n}}\left\{\sum_{m}(A_{nm}F_{nm}^{(\kappa),k+1})+V_{n}q_{n}^{\kappa,k+1}\right\}$$
$$\times(\kappa=1,2,3\text{ and }4) \tag{3}$$

where the superscript κ is an equation or component index, and κ=1, 2, 3, and 4 denote water, air, tracer/solute/radionuclide and heat, respectively. The decay constants, λ_{κ}, are

zero unless κ=3 for a decaying tracer/solute/radionuclide component. The summation in Eq. (3) accounts for mass or energy inflow/outflow contributed within the continuum and/or other continua.

Wu and Pruess (2000) provide detailed formulas for evaluating accumulation (M_n) and flow ($F_{n,m}$) terms for Eq. (3), including how to calculate dispersive (conductive for heat) and advective mass and heat fluxes, respectively. In addition, we extend the MINC approach directly (Pruess, 1983) for handling flow and interactions between large fractures and the matrix. However, this work introduces small fractures as an additional continuum. To evaluate flow terms between small fractures and large fractures or between small fractures and the matrix, we require additional geometric parameters such as the interface areas and characteristic lengths for these connections. In the demonstration examples of this study, small fractures are represented by one cell locally interacting with large fracture and matrix systems (Fig. 3).

Table 1 summarizes the parameters of the equations needed to determine the characteristic distances used in calculating flow between the three continua for the cases of regular one-, two- and three-dimensional large fracture networks, each with uniform distributions of small fractures. The quasi-steady-state flow assumption of Warren and Root (1963) is used to derive the characteristic distances, listed in Table 1, when the matrix is represented by only one gridblock. The flow distance between small fractures (f) and large fractures (F) is taken to be half the characteristic length of the small fractures within a matrix block (Figs. 4 and 5). Furthermore, the interface areas between the small fractures and the matrix (M) are calculated using the geometric data of the small fractures. Interface areas between large fractures and the matrix and between large fractures and small fractures are treated using the geometry of the large fractures. This treatment has implicitly defined the permeabilities of the two fractures in a continuum sense, such that bulk connection areas are needed to calculate Darcy flow between the two fracture continua. In summary, we extend the Warren and Root (1963) approach to evaluate interactions along F–M and f–M connections.

The model formulation (Section 2) is applicable to both single-continuum and multi-continuum conditions. When handling flow and transport through triple-continuum fractured rock, one of the main challenges is to generate a mesh that represents both

Table 1
Characteristic distances[a] for evaluating flow terms between two fracture and matrix systems

Large fracture networks	Dimensions of matrix blocks	Characteristic dimension (m) of large fractures	Characteristic F–M distances (m)	Characteristic dimension (m) of small fractures	Characteristic F–f distances (m)	Characteristic f–M distances (m)
1-D	A	$l_F=A$	$l_{FM}=l_F/6$	$l_f=a$	$l_{Ff}=l_x/2$	$l_{fM}=l_f/6$
2-D	A B	$l_F=(2AB)/(A+B)$	$l_{FM}=l_F/8$	$l_f=2ab/(a+b)$	$l_{Ff}=(l_x+l_y)/2$	$l_{fM}=l_f/8$
3-D	A B C	$l_F=3ABC/(A+B+C)$	$l_{FM}=l_F/10$	$l_f=3abc/(a+b+c)$	$l_{Ff}=(l_x+l_y+l_z)/2$	$l_{fM}=l_f/10$

[a] Note in Table 1, A, B, and C are dimensions of matrix blocks along x, y, and z directions, respectively. Dimensions a, b, and c are fracture-spacings of small fractures along x, y, and z directions, respectively. Subscript F represents large-fracture; f, small-fracture, and M, matrix systems, respectively.

types of fractures as well as the matrix continuum. This triple-continuum, fracture–matrix mesh can be generated based on the MINC concept (Pruess, 1983), i.e., starting from a primary or single-porous medium mesh that uses bulk volume of formation and layering only. Then, we use geometric information of the corresponding two-type fractures within one formation subdomain or one finite-difference gridblock of the primary mesh, and fractures are lumped into the large fracture continuum and small fracture continuum, respectively. The rest is regarded as the matrix continuum. The connection distances and interface areas are calculated accordingly, using the relations listed in Table 1 and the geometric data of the fractures. Once a proper mesh for a triple-continuum system is generated, fracture and matrix blocks are specified to represent fracture or matrix continua, separately.

4. Triple-continuum behavior of flow and transport processes under single-phase flow conditions

In this section, we discuss flow and transport behavior through the triple-continuum model under single-phase conditions (airflow in unsaturated fracture–matrix system or water flow in saturated fractured rocks). Both analytical and numerical approaches are used in this section. Note that this discussion builds on Warren and Root (1963) and Wu and Ge (1983). Although the following analyses are for single-phase water flow conditions, the methodology can be shown to be applicable to single-phase gas flow when using the conventional linearization to the gas-flow governing equation and dimensionless variables. Therefore, they may be applicable to the UZ of Yucca Mountain, because the ambient water flow at the site, relative to gas flow or transport tests, is very slow and can be ignored.

4.1. Analytical solution

To use an analytical approach, we further simplify Eqs. (1) and (2) to a case involving slightly compressible fluid isothermal flow. We also assume that global flow through the matrix system is insignificant. Furthermore, the quasi-steady-state flow assumption is used for flow between a large-fracture continuum and the matrix (F–M), and between a small-fracture continuum and the matrix (f–M). Given these assumptions, the flow in a triple-continuum system can be described as a triple-porosity model.

For flow through large fractures:

$$-\nabla \cdot (\rho \boldsymbol{v}) - \phi_{\mathrm{M}} C_{\mathrm{M}} \frac{\partial P_{\mathrm{M}}}{\partial t} - \phi_{\mathrm{f}} C_{\mathrm{f}} \frac{\partial P_{\mathrm{f}}}{\partial t} = \phi_{\mathrm{F}} C_{\mathrm{F}} \rho_{\mathrm{i}} \frac{\partial P_{\mathrm{F}}}{\partial t} \tag{4}$$

For interacting with small fractures:

$$\phi_{\mathrm{f}} C_{\mathrm{f}} \frac{\partial P_{\mathrm{f}}}{\partial t} = \frac{\alpha_{\mathrm{Ff}} k_{\mathrm{f}}}{\mu} (P_{\mathrm{F}} - P_{\mathrm{f}}) + \frac{\alpha_{\mathrm{fM}} k_{\mathrm{M}}}{\mu} (P_{\mathrm{M}} - P_{\mathrm{f}}) \tag{5}$$

For interacting with the matrix:

$$\phi_M C_M \frac{\partial P_M}{\partial t} = \frac{\alpha_{FM} k_M}{\mu}(P_F - P_M) + \frac{\alpha_{fM} k_M}{\mu}(P_f - P_M) \tag{6}$$

where the shape factor for F–M or f–M is defined by Warren and Root (1963)

$$\alpha_{FM} = \alpha_{fM} = \alpha \tag{7}$$

For F–f interaction, the shape factor for small fractures is defined as

$$\alpha_{Ff} = \frac{A_{Ff}}{l_{Ff}} \tag{8}$$

where A_{Ff} is the total large-fracture and small-fracture connection area per unit volume of rock (m^2/m^3) and l_{Ff} is defined in Table 1 for 1-D, 2-D, and 3-D small fractures, respectively.

The problem under consideration is one-dimensional radial flow into (or out of) a fully penetrating well in a radially infinite, horizontal reservoir that contains uniform fracture and matrix properties. The system is subject to uniform initial pressure and a constant injection/pumping rate at the well. When wellbore storage and skin effects can be ignored, an asymptotic solution for a dimensionless pressure can be derived in terms of dimensionless variables (Liu et al., 2003):

$$P_D(r_D = 1, t_D) = \frac{1}{2}[\ln t_D + 0.80909 + E_i(-A_1 t_D) - E_i(-B_1 t_D) + E_i(-A_2 t_D) - E_i(-B_2 t_D)] \tag{9}$$

where the function E_i is called the exponential integral. Variables A_1, A_2, B_1, B_2, and other dimensionless variables used are defined in Table 2.

According to Warren and Root (1963), flow through a double-porosity medium can be sufficiently characterized by two parameters, storage parameter ω and interporosity parameter λ. The solution in Eq. (9) indicates that the flow in the triple-continuum reservoir is characterized by five dimensionless parameters: 2 ω's and 3 λ's (Table 2). Note that only two of the three ω's are independent. This may increase the difficulty in determining a unique set of fracture–matrix properties, using a parameter estimation approach based on inverse modeling. In an effort to resolve this non-uniqueness issue, the next two sections present a methodology for using well-pressure and tracer tests. These tests, when associated with field and laboratory studies, may provide a possible solution for determining all the model parameters.

4.2. Examination of analytical solutions

In this section, we examine the analytical solution (Eq. (9)) and evaluate its accuracy and applicability to describing transient flow in triple-continuum media, using the numerical simulation results obtained with the TOUGH2 code (Pruess, 1991; Wu et al., 1996).

Table 2
Dimensionless parameters and variables used in the analytical solutions of flow through a triple-continuum reservoir

Parameter	Definition
Dimensionless time	$t_D=k_F t/(\mu r_w^2(\phi_m C_m+\phi_f C_f+\phi_F C_F))$
Dimensionless radius	$r_D=r/r_w$
Dimensionless pressure	$P_D=\dfrac{P_i-P_F(r,t)}{\dfrac{q\mu}{2\pi k_F h}}$
F–M interporosity parameter	$\lambda_{FM}=\alpha_{FM} r_w^2 k_M/k_F$
F–f interporosity parameter	$\lambda_{Ff}=\alpha_{Ff} r_w^2 k_f/k_F$
f–M interporosity parameter	$\lambda_{fM}=\alpha_{fM} r_w^2 k_M/k_f$
F storativity	$\omega_F=\phi_F C_F/(\phi_m C_m+\phi_f C_f+\phi_F C_F)$
f storativity	$\omega_f=\phi_f C_f/(\phi_m C_m+\phi_f C_f+\phi_F C_F)$
M storativity	$\omega_M=\phi_M C_M/(\phi_m C_m+\phi_f C_f+\phi_F C_F)$
Variables based on parameters listed above	
$A_1=A_0+\frac{\lambda_{FM}+\lambda_{Ff}}{2\omega_F}+\left[\left(A_0+\frac{\lambda_{FM}+\lambda_{Ff}}{2\omega_F}\right)^2-\frac{B_0}{\omega_F}\right]^{1/2}$	
$A_2=A_0+\frac{\lambda_{FM}+\lambda_{Ff}}{2\omega_F}-\left[\left(A_0+\frac{\lambda_{FM}+\lambda_{Ff}}{2\omega_F}\right)^2-\frac{B_0}{\omega_F}\right]^{1/2}$	
$B_1=A_0+(A_0^2-B_0)^{1/2}$	
$B_2=A_0+(A_0^2-B_0)^{1/2}$	
$A_0=\frac{1}{2}\left[\frac{\lambda_{FM}}{\omega_M}+\frac{\lambda_{Ff}}{\omega_f}+\left(\frac{1}{\omega_M}+\frac{1}{\omega_f}\right)\lambda_{fM}\right]$	
$B_0=\frac{\lambda_{FM}\lambda_{Ff}+(\lambda_{FM}+\lambda_{Ff})\lambda_{fM}}{\omega_M\omega_f}$	

The verification problem concerns typical transient flow towards a well that fully penetrates a radially infinite, horizontal, and uniformly fractured reservoir. In the numerical model, a radially finite reservoir (r_e=10,000 m) with 20 m thickness, as illustrated by Fig. 6, is used and discretized into a one-dimensional (primary) grid.

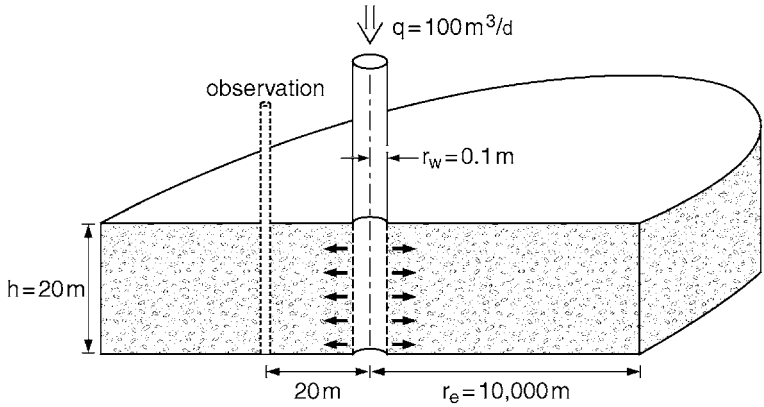

Fig. 6. Schematic illustration of a fully penetrating injection well in a radial, uniform, and horizontal formation used for well flow analyses and tracer tests.

The distance r_e (10,000 m) is subdivided into 2100 intervals following a logarithmic scale. A triple-continuum mesh is then generated from the primary grid, in which the one-dimensional, horizontal large-fracture plate network is assumed to be a uniform disk-shaped matrix block. Fracture and matrix parameters are given in Table 3. Note that the values of these parameters are selected within the typical range of a triple-continuum model (i.e., $k_F\, k_f\, k_M$ and $\phi_M\, \phi_f\, \phi_F$). The properties of large fractures and matrix correspond to those of the Prow Pass Tuff at Yucca Mountain (Wu et al., 2000).

For this problem, many numerical tests and analyses have been performed to confirm the accuracy of these numerical simulation results, and here the numerical solutions are considered to be "exact" solutions (as explained below) for comparison. Fig. 7 presents a comparison of numerical-modeling results (circles) with the approximate analytical solution (Eq. (9), solid-line) using the input parameter values (Table 3). Excellent agreement exists between the two solutions, except for very small differences at very early times (t_D<10). (Here a dimensionless time of t_D=50 corresponds to 1 s). The analytical solution, which is long-time asymptotic and similar to the Warren-Root solution, may not be valid for t_D<100. In addition, the analytical solution may also introduce some errors at early times because it relies on the quasi-steady-state assumption for inter-

Table 3
Parameters used in the single-phase flow problem through the triple-continuum, fractured reservoir

Parameter	Value	Unit
Matrix porosity	ϕ_M=0.263	
Large-fracture porosity	ϕ_F=0.001	
Small-fracture porosity	ϕ_f=0.01	
Large-fracture spacing	A=5	m
Small-fracture spacing	a=1.6	m
F characteristic length	l_x=3.472	m
F–M/F–f areas per unit volume rock	A_{Ff}=0.61	m^2/m^3
Reference water density	ρ_i=1000	kg/m^3
Water phase viscosity	$\mu=1\times10^{-3}$	Pa·s
Matrix permeability	$k_M=1.572\times10^{-16}$	m^2
Large-fracture permeability	$k_F=1.383\times10^{-13}$	m^2
Small-fracture permeability	$K_f=1.383\times10^{-14}$	m^2
Water production rate	q=100	m^3/day
Total compressibility of three media	$C_F=C_M=C_f=1.0\times10^{-9}$	1/Pa
Well radius	r_w=0.1	m
Formation thickness	h=20	m
F–M shape factor	α_{FM}=0.480	m^{-2}
F–f shape factor	α_{Ff}=0.351	m^{-2}
f–M shape factor	α_{Ff}=4.688	m^{-2}
F–M interporosity parameter	$\lambda_{FM}=0.546\times10^{-6}$	
f–M interporosity parameter	$\lambda_{fM}=0.533\times10^{-5}$	
F–f interporosity parameter	$\lambda_{Ff}=0.480\times10^{-4}$	
F storativity	ω_F=0.0036	
f storativity	ω_f=0.0365	
M storativity	ω_M=0.9599	

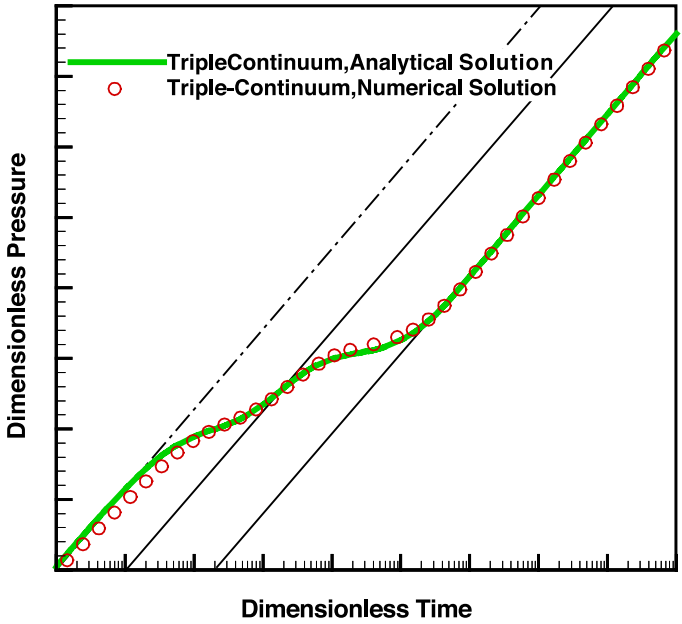

Fig. 7. Typical behavior curve of flow through a triple-continuum fracture medium, showing three-parallel semi-log straight lines from effects of three continua.

continuum flow (Kazemi, 1969), which is not satisfied during the early rapid transient flow. Furthermore, the analytical solution ignores the effect of global matrix–matrix flow, which is included in the numerical solution. Therefore, the numerical solution is considered to be more accurate for early time behavior (Fig. 7).

Many additional modeling comparisons have been performed using different parameter sets. In all cases, the analytical solution of Eq. (9) was found to be very accurate for describing slightly compressible fluid flow through a triple-continuum system. Note that the numerical model used in this study includes global connections for the matrix continuum. Fig. 7 shows that ignoring matrix–matrix connections is a good approximation under single-phase flow conditions with normal fractured medium properties. In addition, we have examined the effect of matrix–matrix connections by comparing the Warren-Root analytical solution with double-porosity and dual-permeability numerical model results. All the comparisons indicate that matrix–matrix connections can be ignored for single-phase flow.

4.3. Discussion and application of the analytical solutions

The curve in Fig. 7 exhibits three distinct, straight, parallel lines in semi-log space. This is typical behavior for flow through the triple-continuum model and is similar to flow through a triple-porosity model (Wu and Ge, 1983). The first straight line, occurring at a very early time, represents pressure responses to flow in high-permeability large fractures near the well. The second line (at intermediate times) reflects the effects on flow of fluid

storage in secondary permeable, small fractures. In contrast, the third straight-line portion (which corresponds to later-time flow behavior) is controlled by the high-storage, low-permeability matrix. However, depending on the fracture and matrix properties, as well as wellbore conditions (e.g., storage and skin effects), the first straight line may not develop or may occur too soon to be measured in a well test, if the large-fracture porosity is very small.

The analytical solution (Eq. (9)) and the basic pattern of flow in triple-continuum media (Fig. 7) suggest that it is possible to estimate small-fracture properties using traditional well-test techniques, if at least two semi-log straight lines develop in a pressure drawdown or buildup curve. Taking advantage of a property of the exponential integral, E_i function:

$$E_i(x) \approx \ln(x) + 0.5775 \qquad (x < 0.0025) \tag{10}$$

we can determine the four parameters, A_1, A_2, B_1, and B_2 (Table 2), subject to the condition:

$$A_1 > B_1 > A_2 > B_2 \tag{11}$$

Fig. 8 defines several parameters: vertical distances (displacements) between the three semi-log straight lines (δP_{FM}, δP_{Ff}, δP_{fM}) and two pressure drops (P^*_{Ff} and P^*_{fM}) at transitional points between the semi-log straight lines. Applying Eqs. (10) and (11) to Eq.

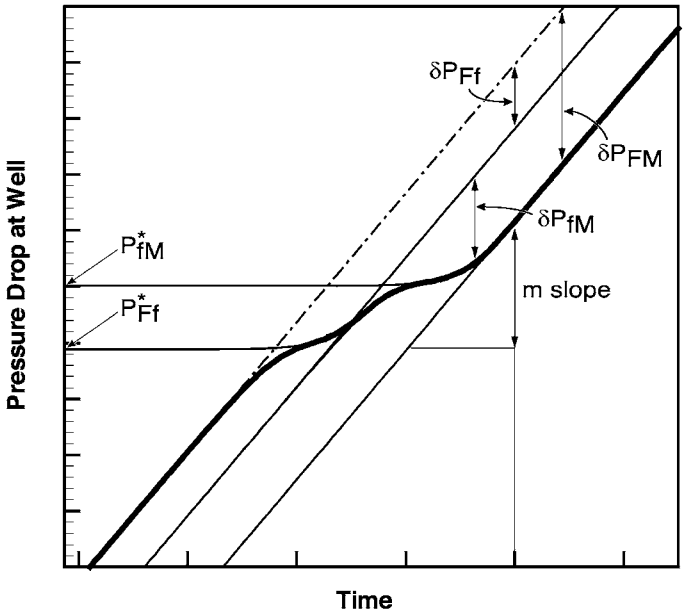

Fig. 8. Schematic of pressure testing curves of flow through a triple-continuum fractured media, defining vertical distances and transitional point pressures for well-test analyses.

(9) and using analysis methods analogous to those previously used for a double-porosity model (Earlougher, 1977), we derive the following expressions for estimating small-fracture porosity:

$$\omega_F \approx \exp(-\delta P_{FM}/m) \tag{12}$$

$$\frac{\phi_F C_F}{\phi_f C_f + \phi_F C_F} \approx \exp(-\delta P_{Ff}/m) \tag{13}$$

$$\frac{\phi_f C_f}{\phi_f C_f + \phi_M C_M} \approx \exp(-\delta P_{fM}/m) \tag{14}$$

where m is the slope of the semi-log straight line (Fig. 7), defined as:

$$m = \frac{q\mu}{4\pi k_F h} \tag{15}$$

Similarly, we have the following relations for calculating small-fracture permeability:

$$\ln\left(\frac{A_2}{B_0}\right) + 0.2319 \approx P^*_{Ff}/m \tag{16}$$

and

$$-\ln B_2 + 0.2319 \approx P^*_{fM}/m \tag{17}$$

Using the parameters listed in Table 3, we have confirmed that Eqs. (12)–(17) give good estimates for small-fracture properties. Eq. (15) can be used to estimate the permeability of large fractures, as long as a late-time semi-log straight line develops from a pressure drawdown or buildup curve from a well test.

Compared with small fractures, matrix and large-fracture properties are relatively easy to determine in the field, using core samples of matrix rock and pneumatic or air-k data, respectively. Eqs. (12)–(17) provide a methodology for estimating small-fracture parameters from well-pumping (or injection) testing data under known matrix and large-fracture properties. Note that if only the second and third straight line develops, we can use Eqs. (14) and (17) to estimate small-fracture properties.

4.4. Tracer transport behavior under single-phase flow conditions

In this section, we study the transport behavior of a conservative tracer under single-phase conditions using a numerical simulator, the T2R3D code (Wu et al., 1996). The fracture–matrix system under consideration is identical to the one-dimensional radial-flow problem (Fig. 6) of Section 4.2. However, here we use both the triple-continuum and dual-permeability methods described above for comparison purposes. The transport problem is defined as a single-well tracer test with a pulse-

tracer injection lasting 5 days. Throughout the numerical tracer test, the flow remains at a steady-state condition with a volumetric well injection rate maintained at 100 m^3/day. The fracture and matrix properties and fluid parameters used are also given in Table 3, with the exception that fracture properties in the dual-permeability model correspond to those for large fractures. In addition, we specifically select two scenarios to study the effect of fracture porosity in the two models. In the first scenario, fracture porosity for the dual-permeability model ($\phi_{f,2k}$=0.0011) is set to be equal to the summation of the large-fracture and small-fractures porosities (ϕ_F=0.000264 and ϕ_f=0.000836) of the triple-continuum model. In the second scenario, fracture porosity ($\phi_{f,2k}$=0.001) in the dual-permeability model is set equal to the large-fracture porosity (ϕ_F=0.001) in the triple-continuum model. In both cases, we ignore mechanical dispersion effects. The molecular diffusion coefficient for the tracer is 1.6×10^{-10} m^2/s, and tortuosity for the three continua is 0.7.

Fig. 9a shows tracer breakthrough curves, "observed" at a location of 20 m away from the well, for the first scenario. In this case, the triple-continuum model predicts a much earlier breakthrough time than the dual-permeability model. This is because the solute transport is dominated by advection for the test problem on the time scale concerned. The flow along large fractures in the triple-continuum model is much faster than that through the fractures in the dual-permeability model [$\phi_{f,2k}$(=0.0011) >ϕ_F(=0.000264)]. In addition, interflow between different continua in both models tends to be very small under steady-state single-phase flow conditions. Consequently, small fractures affect overall transport behavior through diffusion only, which is a much slower process than advection.

For the second scenario ($\phi_{f,2k}$=ϕ_F=0.001), the breakthrough curves from the two models are almost identical (Fig. 9b). This is because the system is still dominated by advection, and the global fracture flow rates are very similar in the two models. In our simulations, we also reduced the well water injection rate by two orders of magnitude and increased the molecular diffusion coefficient (these results are not shown in figures). In those cases, the triple-continuum model gives a slightly later breakthrough time than the dual-permeability model. This difference results from the enhanced diffusion into the matrix (with the triple-continuum model) through the small fractures.

The tracer breakthrough curves (Fig. 9a,b) show the sensitivity to the fracture porosities in the triple-continuum model. This suggests that tracer tests may provide additional information regarding small-fracture porosity. For example, the tracer breakthrough curve can be used to distinguish contributions of large and small fractures to the measured total fracture porosity. In practice, however, the determination of the complete model parameters may be possible only when combining well pressure

Fig. 9. (a) Breakthrough curves of relative tracer concentration at 20 m from the well for the scenario of dual-permeability model fracture porosity equal to combined porosity of large and small fractures in a triple-continuum model. (b) Breakthrough curves of relative tracer concentration at 20 m from the well for the scenario of a dual-permeability model fracture porosity equal to large-fracture porosity with a triple-continuum model.

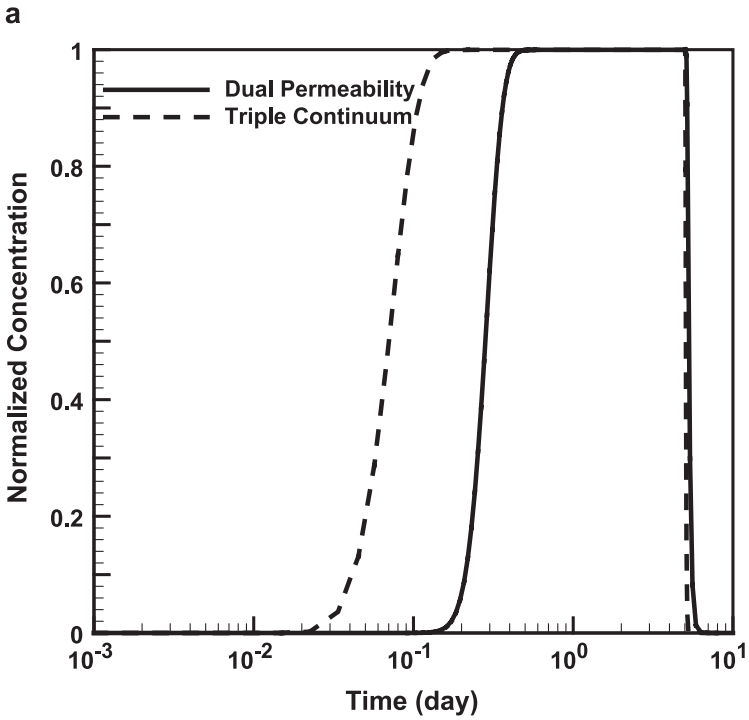
a
Dual Permeability
Triple Continuum
Normalized Concentration
Time (day)
0
0.2
0.4
0.6
0.8
1
10-3
10-2
10-1
100
101

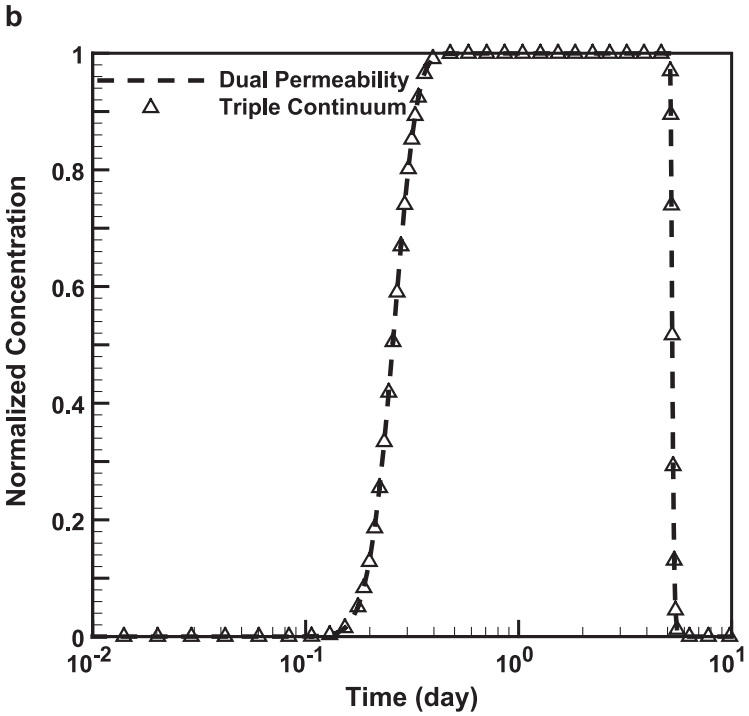
b
Dual Permeability
Triple Continuum
Normalized Concentration
Time (day)
0
0.2
0.4
0.6
0.8
1
10-2
10-1
100
101

and tracer tests with field (e.g., fracture mapping) and laboratory (e.g., matrix properties) studies.

5. Model application: effects of small fractures on flow and transport in the UZ at Yucca Mountain

In this section, we will apply the proposed triple-continuum model to studying flow and transport processes in the UZ of Yucca Mountain. Special attention is given to the potential effects of small fractures on UZ flow and transport. Here, we present two application examples: (1) parameter estimation using field observation data and inverse-modeling studies and (2) three-dimensional mountain-scale flow and transport simulations.

5.1. Hydrogeologic setting

The UZ of Yucca Mountain, 500–700 m thick, overlies a relatively flat water table in the vicinity of the potential repository area. The proposed repository would be located in the highly fractured Topopah Spring welded unit, more than 200 m above the water table. Yucca Mountain is a structurally complex system of Tertiary volcanic rock, consisting of alternating layers of welded and nonwelded ash-flow and air-fall tuffs. The primary geologic formations at Yucca Mountain (beginning from the land surface) consist of the Tiva Canyon, Yucca Mountain, Pah Canyon, and Topopah Spring tuffs of the Paintbrush Group. Underlying these are the Calico Hills Formation, and the Prow Pass, Bullfrog, and Tram tuffs of the Crater Flat Group (Buesch et al., 1995).

These geologic formations have been reorganized into several hydrogeologic units, based primarily on their degree of welding (Montazer and Wilson, 1984). These are the Tiva Canyon welded (TCw) hydrogeologic unit, the Paintbrush nonwelded (PTn) unit, the Topopah Spring welded (TSw) unit, the Calico Hills nonwelded (CHn) unit, and the Crater Flat undifferentiated (CFu) unit. Fig. 10 shows a plan view of the site-scale UZ model grid, including the model domain, borehole locations, and the faults incorporated into the Yucca Mountain model.

5.2. Parameter estimation

To model flow and transport in the UZ using the triple-continuum model, we need to estimate the hydraulic properties for both types of fractures and rock matrix. In Section 4.3, we developed an approach to estimate small-scale fracture properties, based on observations of single-phase flow (airflow in unsaturated or water flow in saturated fracture–matrix systems). However, the small-scale fracture property data determined using this approach are not currently available for different hydrogeological units. In this section, we present a methodology to estimate small-scale fracture properties based on inverse modeling (Banddurraga and Bodvarsson, 1999). Because of data limitations, a number of assumptions are made to demonstrate application of the proposed model.

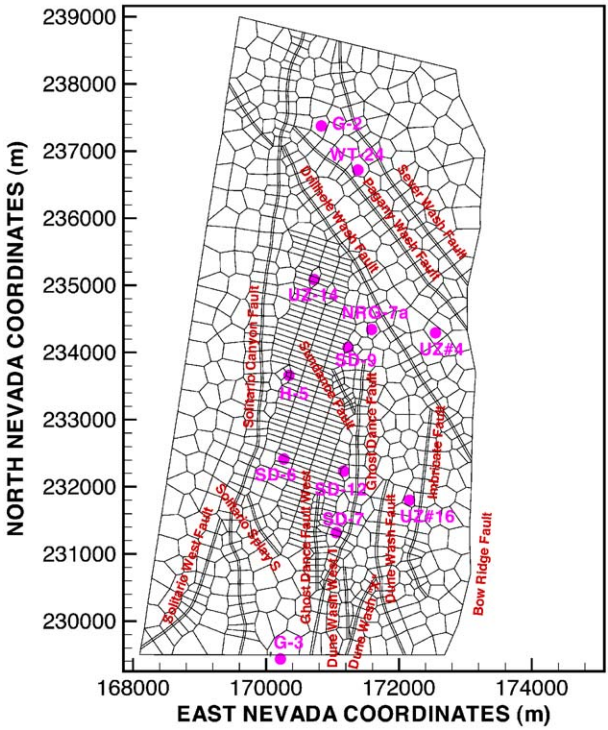

Fig. 10. Plan view of the 3-D UZ model grid, showing the model domain, faults incorporated, and borehole locations at Yucca Mountain.

Analysis of fractures mapped from the Tptpmn unit (Figs. 1 and 2) and two other adjacent units resulted in the following relations for the Tptpmn unit:

$$\frac{d_f}{d_F} = 3.13 \tag{18a}$$

$$\frac{SP_f}{SP_F} = 0.32 \tag{18b}$$

$$\frac{L_f}{SP_f} = 2.17 \tag{18c}$$

where d, SP, and L refer to scanline fracture density (fractures/m), average fracture spacing (m), and average trace length of fractures (m), respectively. As before, the subscripts F and f refer to large-scale and small-scale fractures, respectively. Here we assume that large-scale fractures are longer than 0.51 m, as reported in Liu et al. (2000). The value of this "critical trace length" was determined empirically at Yucca Mountain (Liu et al., 2000). (To better distinguish between large-scale and small-scale fractures, more rigorous

methods need to be developed in future studies.) We further assumed that the porosities of the large-scale and small-scale fractures are proportional to their scanline densities (d_f and d_F). The total fracture porosity, as determined using available gas tracer data (Liu et al., 2000), is considered to include both large and small fractures for the triple-continuum model.

Because most of the geological units do not have mapped small-fracture data, we assume that Eqs. (18a)–(18c) and the method discussed above can be used to estimate the fracture porosities for both large-scale and small-scale fractures for the other units. Note that the primary objective of this study is to evaluate the relative impact of small fractures on the flow and transport processes in the Yucca Mountain UZ. Since values for total fracture porosity, large-scale fracture spacing, and large-scale fracture density are now available for all the geologic units (Liu et al., 2000), the corresponding small-scale fracture properties can be easily determined. These property values are also needed for generating triple-continuum numerical grids.

Unsaturated flow in fractures is commonly characterized by fingering flow at different scales. This flow mechanism must be considered in order to accurately model flow and transport in fractured rock. Recently, Liu et al. (1998) proposed an active fracture model that incorporates fingering flow into the continuum approach. The active fracture model was used in this study to describe flow and transport in fractures. Liu et al. (1998) divided the fracture continuum into two parts, active and inactive, to account for the fingering flow at the fracture-network scale. Flow and transport occurs only within the active fracture continuum, while the inactive part is simply bypassed. The portion of active fracture continuum relative to the whole fracture continuum (f_a) is dynamic and assumed to be a power function of effective saturation (S_e) within the fracture continuum (Liu et al., 1998):

$$f_a = S_e^{\gamma} \tag{19}$$

where γ is a constant (active fracture parameter). The active fracture model can be used for both the large-scale fracture continuum and the small-scale fracture continuum. For simplicity, we further assume that the two kinds of fracture continua have the same γ value.

As a result of fingering flow at different scales, the effective interface area between fractures and the matrix is considerably smaller than the geometric interface area (Liu et al., 1998). The ratio of the effective interface area to the geometric interface area is called the interface area reduction factor (R). Interface-area reduction also exists for interfaces between large-scale and small-scale fractures and between small-scale fractures and the matrix. The R expression for the interface between large-scale fracture and the matrix is given by Liu et al. (1998). It includes the effects stemming from the differences between active fracture spacing and geometric fracture spacing as determined from fracture maps. The pure reduction factor for interface area between large-scale fractures and the matrix, without considering the effects of differences between fracture spacings, is (Liu et al., 1998)

$$R = S_e \tag{20}$$

where S_e is the effective saturation in large-scale fractures. Because the interface area between large-scale and small-scale fractures is proportional to the interface area between

large-scale fractures and the matrix (Fig. 5), the R expression defined in Eq. (20) can be used for the interface between the two kinds of fractures. (In this case, the effective saturation for the large-scale fractures should be used for calculating R.) Following the same logic used to derive Eq. (20) (Liu et al., 1998), this equation can also be used for the interface between small-scale fractures and the matrix, as long as the effective saturation applies to the small-scale fractures.

The determination of hydraulic properties for small-scale fractures (using inverse modeling) involves matching 1-D simulation results to observed data collected from various boreholes (Fig. 10). In this study, matrix saturation and water-potential data collected from boreholes SD-12 and UZ-14 were used in the inversion. The properties determined from the inverse modeling are permeability and van Genuchten (1980) α (a measure of air entry value) for the small fractures in all the units. The other properties, such as relative permeability, are assumed to be the same as those for the large-scale fractures. During the inversion, properties for the matrix and large-scale fractures are set in accordance with the calibrated values given in Ahlers and Liu (2000). Fig. 11 shows the comparison between simulated and observed matrix saturation distributions for a vertical column corresponding to borehole SD-12. As expected, the estimated permeability and α values for the small fractures generally fall between the values for the large-scale fractures and the matrix. For example, Table 4 shows the estimated small-scale-fracture properties for the Tsw34 unit as an example, compared with those for the matrix and the large-scale fractures. Estimated parameters are used in all the triple-continuum simulations described in the following sections.

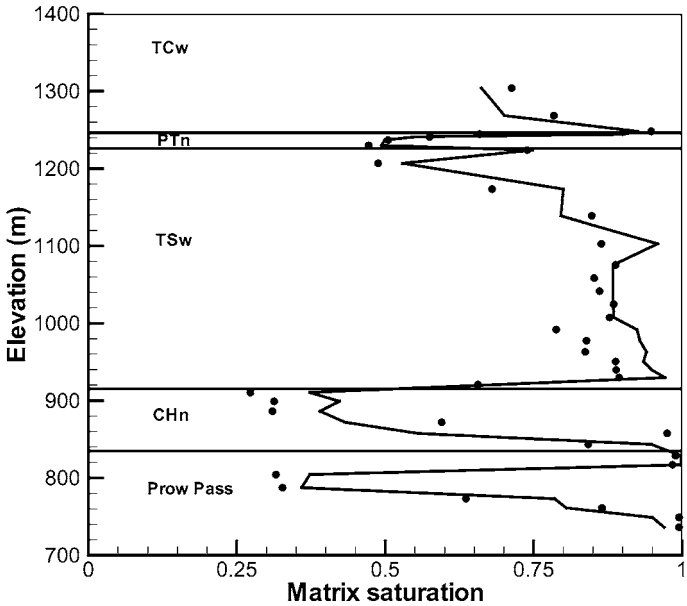

Fig. 11. Comparison between the matrix water-potential profile for the submodel corresponding to borehole SD-12 (solid line, obtained from inverse modeling) and the measured data (black circles).

Table 4
Small fracture properties for Tsw34

	Matrix	Small fracture	Large fracture
Permeability (m^2)	4.07e−18	5.02e−16	1.70e−11
Van Genuchten α (Pa^{-1})	3.86e−6	3.16e−4	5.16e−4

5.3. 3-D flow and transport simulations

The three-dimensional modeling studies described in this section are based on the current 3-D site-scale UZ flow model (Wu et al., 2000). The aerial domain of the UZ model encompasses approximately 40 km^2 of the Yucca Mountain area (Fig. 10). The 3-D UZ model grid, as shown in Fig. 10, has 1324 mesh columns consisting of both fracture and matrix continua and 37 vertical computational grid layers, resulting in a total of 145,640 gridblocks and 492,098 connections for the triple-continuum grid.

Fracture–matrix interactions in the 3-D modeling are handled using the triple-continuum methodology and are compared with results from the dual-permeability model. When applied to this study, the two fracture–matrix conceptual models are further modified by the active-fracture model of Liu et al. (1998), as discussed in Section 5.2. For model boundary conditions, the top model boundary is specified as the ground surface of the mountain; the bottom boundary lies at the water table level. Both top and bottom boundaries are Dirichlet-type, while all of the lateral boundaries (Fig. 10) are no-flow (laterally closed). In addition, net surface infiltration is applied to fracture blocks directly below the top boundary as source terms using the present-day, steady-state mean infiltration map, which is spatially varying and was previously estimated by the US Geological Survey (USGS) scientists (Hevesi and Flint, 2000) for the site.

Properties for large fracture and matrix used for the triple-continuum model are the same as those for the dual-permeability UZ flow model (Wu et al., 2000), and small-fracture properties are estimated in Section 5.2. In addition, the present triple-continuum model incorporates the permeability-barrier model to include the occurrence of perched water, as observed in the UZ. The rock properties designated in the triple-continuum model for the perched-water layers/zones are derived from the calibrated permeabilities for these areas (Wu et al., 2000).

Simulation results for steady-state UZ flow using the triple-continuum model are compared with (1) measured moisture data and (2) observed perched-water bodies. For brevity, we show the model comparisons with observed data from boreholes SD-7, SD-9, SD-12, and UZ-14 (Fig. 12). Fig. 12 shows that the modeled results from the triple-continuum simulation are in good agreement with both the measured saturation and the perched water elevations.

Figs. 13 and 14 show the percolation fluxes (fracture flux+matrix flux) at the repository and water table levels, respectively, as simulated by the triple-continuum model. When comparing these results with those obtained using a dual-permeability model (Wu et al., 2000) under the same infiltration scenario and boundary conditions, we find that the total flow patterns for the two models are similar. This may indicate that small fractures have an insignificant impact on global steady-state UZ flow because they are not globally

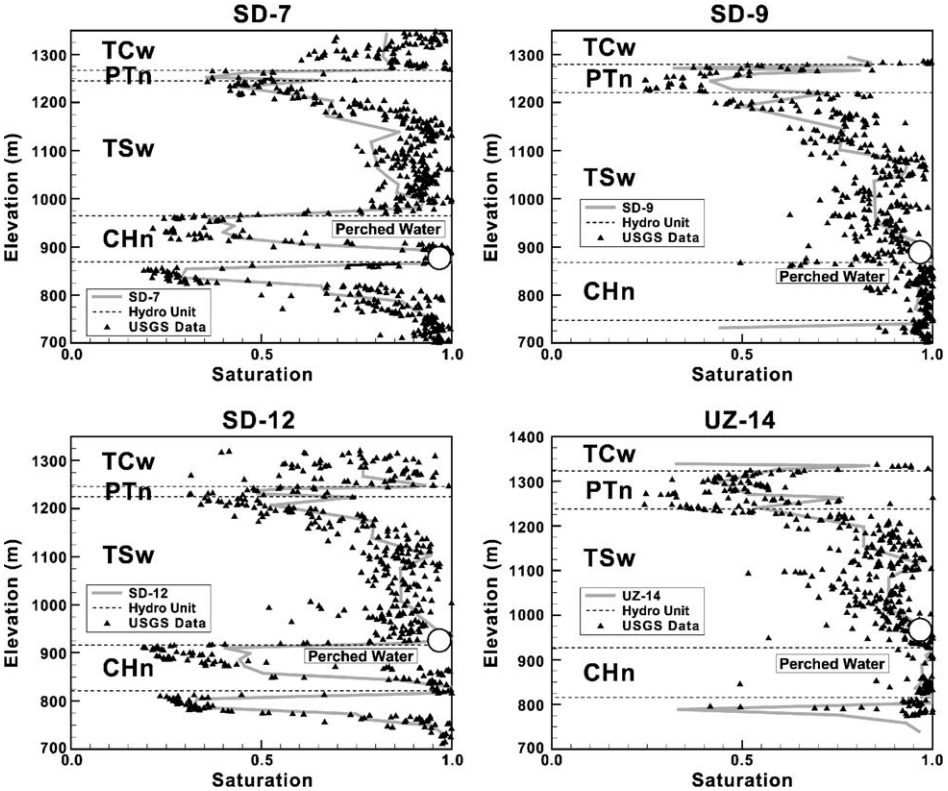

Fig. 12. Comparison of the simulated and observed matrix liquid saturations and perched-water elevations for boreholes SD-7, SD-9, SD-12, and UZ-14, using the triple-continuum model-simulation results with present-day, mean infiltration rate (with the thin-dashed lines representing interfaces between hydrogeological units).

connected. Note that large-fracture and matrix properties used in the triple-continuum model are the same as those for fractures and matrix in the dual-permeability model. This may also contribute to the similarity between the two model results. In general, it is expected that small fractures have less significant impact on *global* steady state flow patterns than on transient flow under both saturated and unsaturated flow conditions.

In addition to the flow simulations for the triple-continuum model, we present model results for the transport of radionuclide tracers under a steady-state 3-D flow field. Transport simulations are conducted for both conservative and reactive tracers, using a decoupled version of the T2R3D code (Wu and Pruess, 2000). The 3-D steady-state flow field, discussed above, is directly used as an input to the T2R3D code for transport runs.

We consider two types of radionuclides: technetium (a conservative tracer) and neptunium (a reactive tracer). The initial conditions for the tracer-transport simulations correspond to the ambient moisture conditions achieved when the flow field reaches the steady state. The two radionuclides are treated as nonvolatile and are transported through the liquid phase only. Radioactive decay and mechanical dispersion effects are ignored. A

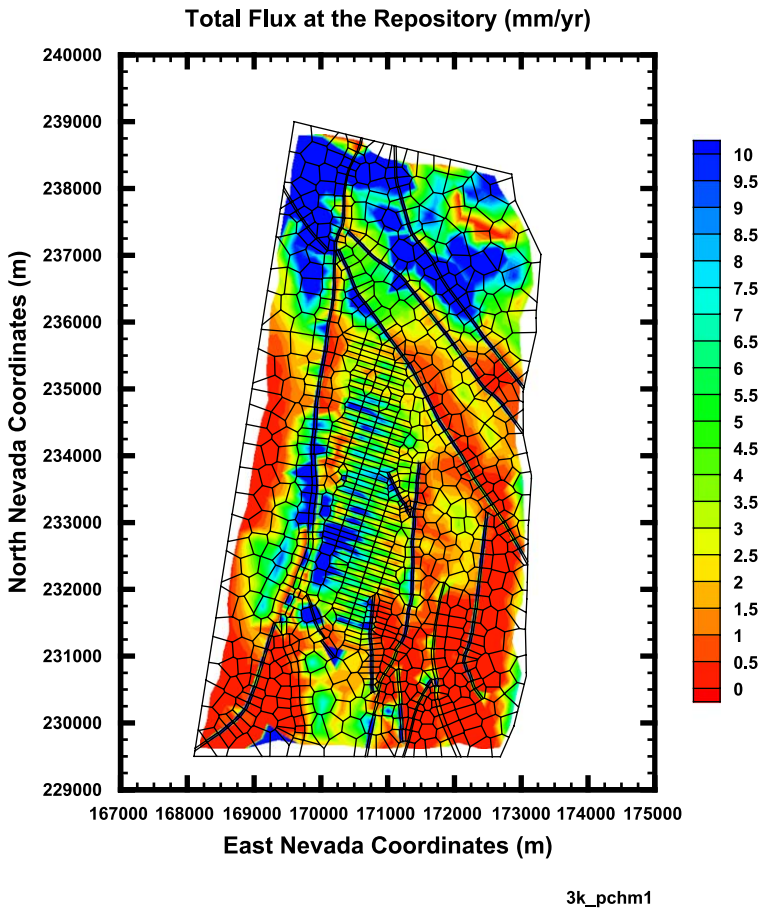

Fig. 13. Simulated percolation fluxes at the repository level under the present-day, mean infiltration rate using the triple-continuum model.

constant molecular diffusion coefficient of 3.2×10^{-11} (m^2/s) is used for diffusion of the conservative component, and a diffusion coefficient of 1.6×10^{-10} (m^2/s) is used for the reactive component. For the adsorbing tracer, several partitioning coefficient (K_d) values are used (Table 5). All transport simulations were run to 1,000,000 years under conditions of steady-state flow and uniform, initial distribution of source concentration at the repository fracture blocks.

Tracer-transport behavior in the UZ is analyzed using a cumulative or fractional breakthrough curve, as shown in Fig. 15 for the present-day mean infiltration scenario. The fractional mass breakthrough in these figures is defined as the cumulative mass of the tracer (radionuclide) arriving at the entire bottom model boundary over time, normalized by the total initial mass of the tracer present at the repository. Fig. 15 compares simulation results from the dual-permeability and triple-continuum models and shows a significant difference between the simulated breakthrough curves. For example, a one-order-of-

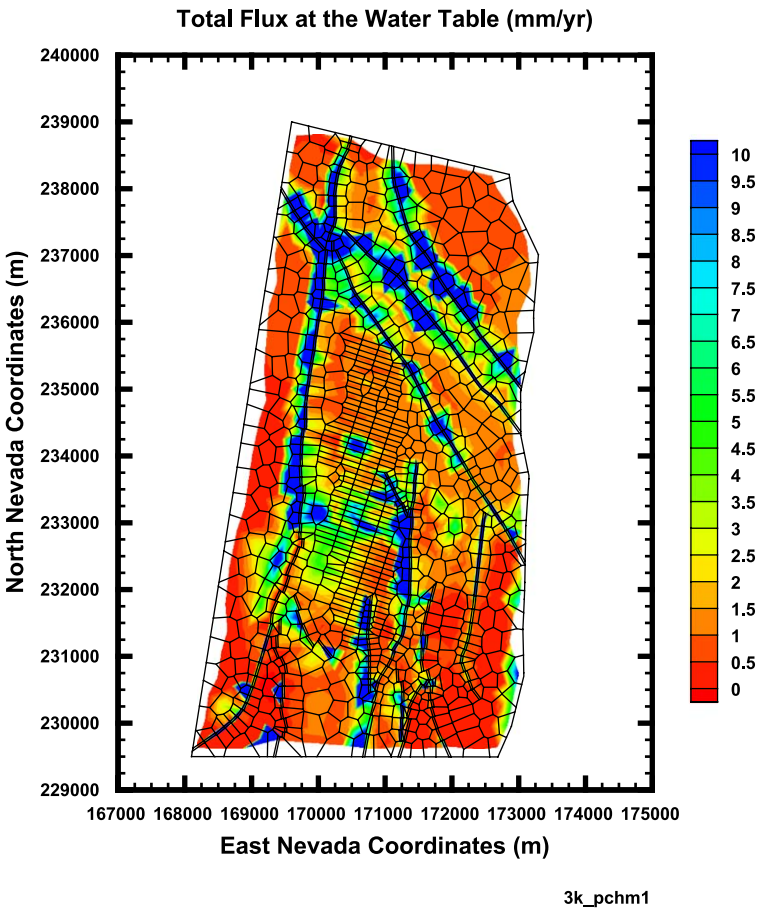

Fig. 14. Simulated percolation fluxes at the water table under the present-day, mean infiltration rate using the triple-continuum model.

magnitude difference appears at the time of 20% mass breakthrough for the nonsorbing radionuclide, Tc. Even for the sorbing radionuclide, Np, at 20% breakthrough times, predicted by the triple-continuum model, are twice those shown for the dual-permeability model.

Table 5
K_d values used for a reactive tracer transport in different hydrogeologic units (Wu et al., 2000)

Hydrogeologic unit	K_d (cm^3/g)
Zeolitic matrix in CHn	4.0
Vitric matrix in CHn	1.0
Matrix in TSw	1.0
Fault matrix in CHn	1.0
Fractures and matrix in the rest of units	0.0

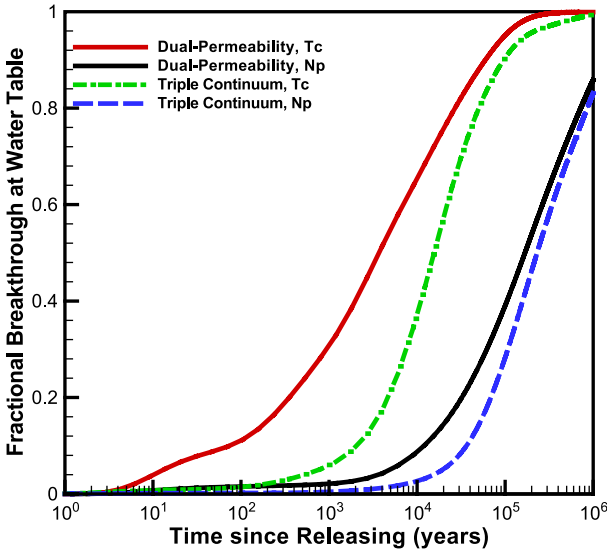

Fig. 15. Comparison between cumulative breakthrough curves at the water table, simulated for conservative and reactive tracer transport from the repository with the dual-permeability and triple-continuum 3-D models, respectively.

The previous dual-permeability modeling studies of Wu et al. (2000) show that the factors that have the most important impact on tracer-transport times are surface infiltration rates, climate scenarios, and sorption effects. The transport results in Fig. 15 indicate that the conceptual model for fracture–matrix interactions is also a very important factor and should be selected appropriately. Note that Fig. 15 shows much longer transport times from the triple-continuum model compared to those from the dual-permeability model. This behavior of predicted breakthrough times is entirely different from transport in the single-phase, triple-continuum medium of Section 4.4, in which the triple-continuum model predicted breakthrough times to be the same or less than those from the dual-permeability model. This difference results primarily from the nature of unsaturated flow in the present triple-continuum simulation. The simulation results show that considerable flow still occurs locally between the large and small fractures and between small fractures and the matrix, even under steady-state conditions. In contrast, little interaction between fracture–matrix systems can occur under single-phase, steady-state flow conditions. Secondly, the percolation fluxes with the 3-D model are much slower than the 1-D radial flow at the well, mainly because of the low infiltration rates at the site (several millimeters per years for the present-day climate). Therefore, diffusion plays a much more important role in the 3-D UZ transport result. In summary, because the triple-continuum model features a stronger interaction between the fractures and the matrix by both advection and diffusion, it predicts much longer transport times at the Yucca Mountain site.

The above discussion is consistent with the findings of Bodvarsson et al. (2001) and Liu et al. (2003). Both of those studies indicate that matrix diffusion and other mechanisms

related to solute transfer between the fractures and the matrix are the important factors controlling overall solute transport behavior within the UZ. In their study, Liu et al. (2003) would need to increase the fracture–matrix interface area in their dual-permeability model to match the field observed breakthrough curve. This increase in area is equivalent to accounting for the effect of small fractures, which show a significant impact on solute transport (Fig. 15).

6. Discussion

In a fracture–matrix continuum containing both large-scale globally connected fractures and small-scale locally connected fractures, the main role played by the small fractures is to control fracture–matrix interflow and transport processes by enlarging effective fracture–matrix interface areas and offering intermediate storage space. Therefore, the small-fracture conceptual model takes into account that dynamic interaction between small fractures and matrix may last hundreds and thousands of years at the Yucca Mountain UZ. Under this conceptualization, small fractures act much faster in response to changes in large fractures than the matrix, since small fractures have much (orders of magnitude) larger permeability than the matrix. In general, the effect of small fractures on flow and transport through fractured rock cannot be simply represented by a dual-permeability model with an increase in fracture–matrix interface areas, which would force an unphysical instantaneous equilibrium between small fractures and the matrix. The example problems of transient well testing, tracer transport, and site-scale radionuclide migration in Sections 4 and 5 indicate that the transient effects of small fractures on flow and transport in these cases are significant and cannot in general be ignored.

Favorable conditions for the triple-continuum model include a typical range of fracture matrix parameters, i.e., $k_F k_f k_m$ and $\phi_m \phi_f \phi_F$. Otherwise, if small-fracture permeability is similar to matrix permeability or very few small fractures exist (i.e., the small-fracture porosity is near zero), the triple-continuum model collapses to a dual-permeability model. Under such conditions, the traditional dual-continuum model should be used instead. On the other hand, if small fractures are extensive and well connected to larger fractures, fracture–matrix equilibrium will be reached relatively quickly, and the fractured system may behave as a single porosity.

Introducing the additional continuum in the triple-continuum model (from the dual-continuum model) requires one more fracture–matrix property set for small fractures. This additional property set makes the triple-continuum model more difficult to use than a dual-continuum model (e.g., Warren and Root model). Furthermore, the complicated flow and transport behavior, as shown in the example problems, indicates that there may be more levels of non-uniqueness in explaining inverse-model results from the triple-continuum model. In an effort to resolve the non-uniqueness issue in determining model parameters, we derived several well-testing analysis equations for estimating small-fracture properties using transient well-testing techniques. In addition, tracer transport under single-phase flow conditions was found to provide an effective estimation of fracture porosity. The methods with well-controlled flow and transport tests, combined

with other field tests (e.g., using air-k tests for large fracture properties and laboratory sample analysis for matrix properties) may provide a possible method for estimating a complete set of fracture–matrix properties.

7. Summary and concluding remarks

We have developed a triple-continuum conceptual model for modeling flow and transport through heterogeneous fractured rock. The model has been implemented into both analytical and numerical approaches. Several theoretical studies were performed with the triple-continuum conceptual fracture model, indicating that transient single-phase flow through a triple-continuum formation can be characterized by three parallel, straight lines on semi-log plots of pressure versus time at a testing well.

The proposed triple-continuum model was used for field sensitivity studies of flow and transport in UZ at Yucca Mountain. First, we applied the new conceptual model to estimate model-related fracture–matrix parameters, using field observation data and an inverse-modeling approach. Then, we incorporated the estimated parameters into the triple-continuum model and performed 3-D site-scale flow and transport simulations, using the current hydrogeological conceptual model of Yucca Mountain.

The triple-continuum modeling results for UZ flow and transport at Yucca Mountain indicate that small fractures may have a significant impact on radionuclide transport in the Yucca Mountain UZ system. Even though the triple-continuum model predicts very different local fracture–matrix interaction from the traditional dual-permeability concept, resultant global, steady-state, unsaturated flow patterns are very similar from one modeling approach to the other.

Nomenclature

a small-fracture spacing along large fracture or the x-direction (m)
A large-fracture spacing along large fracture or the x-direction (m)
A_0, A_1, A_2 parameters for the analytical solution (Table 2)
A_{Ff} total combined area of large fracture and small fracture connections per unit volume of rock (m^2/m^3)
A_{nm} interface areas between two elements n and m (m^2)
b small-fracture spacing along large-fracture or the y-direction (m)
B large-fracture spacing along large-fracture or the y-direction (m)
B_0, B_1, B_2 parameters for the analytical solution (Table 2)
c small-fracture spacing along large fracture or the z-direction (m)
C large-fracture spacing along large fracture or the z-direction (m)
C_{f} total compressibility in small-fracture continuum (Pa^{-1})
C_{F} total compressibility in large-fracture continuum (Pa^{-1})
C_{M} total compressibility in matrix continuum (Pa^{-1})
d_{f} large-fracture density (fractures/m)
d_{F} small-fracture density (fractures/m)

d_m molecular diffusion coefficient (m^2/s) of a component in a fluid phase
$\underline{D}_\beta^\kappa$ effective hydrodynamic dispersion tensor accounting for both molecular diffusion and mechanical dispersion for component κ in phase β (m^2/s)
f denotes small fracture
F denotes large fracture
f_a reduction factor of fracture–matrix interfaces
$F_{nm}^{(\kappa),k+1}$ flow components of mass (κ) ($kg/s/m^2$) or energy (W/m^2) flow along connection nm of time level k+1
h thickness of formation (m)
h_β specific enthalpy of phase β (J/kg)
h_β^κ specific enthalpy of component κ in phase β (J/kg)
k_F absolute permeability of large fracture continuum (m^2)
k_f absolute permeability of small fracture continuum (m^2)
k_M absolute permeability of matrix continuum (m^2)
K_d^κ distribution coefficient of component κ between the liquid phase and rock solids of fractures and matrix (m^3/kg)
K_{th} rock thermal conductivity (W/m °C)
l_f, l_F characteristic length (m) of small and large fractures in the x-direction and y-direction, respectively
l_{Ff}, l_{FM}, l_{fM} characteristic distance (m) between F–f, F–M, and f–M, respectively (defined in Table 1)
L_f average trace length of small fractures (m)
l_x, l_y half-length (m) of small fractures, respectively (defined in Table 3 and illustrated in Figs. 4 and 5)
m slope of semi-log straight lines of pressure versus time curves
M denotes matrix
$M_n^{\kappa,k+1}$ accumulation terms for mass component (κ) (kg/m^3) or energy (J/m^3) of gridblock n at time level $k+1$
P_D dimensionless pressure in fracture continuum
P_j pressure (Pa) in continuum j (j=F, f, and M)
P_{Ff}^*, P_{fM}^* measured pressures (Pa) at transitional points between large fracture to small fracture and between small fracture to matrix, respectively
δP_{FM}, δP_{Ff}, δP_{fM} vertical pressure distances (displacements) (Pa) of three semi-log straight lines, between first and third, first and second, and second and third straight lines, respectively
q^E source/sink or fracture–matrix interaction terms for energy (W/m^3)
q^κ source/sink or fracture–matrix interaction of mass for component κ ($kg/s\ m^3$)
$q_n^{\kappa,\ k+1}$ source/sink or fracture–matrix exchange terms for component κ at element n ($kg/s\ m^3$) of time level k+1
R fracture–matrix area reduction factor
$R_n^{\kappa,\ k+1}$ residual term of mass balance of component (kg/m^3) and energy (J/m^3) balance at element n of time level k+1
r_w well radius (m)
S_e effective liquid saturation
S_β fluid saturation of phase β

SP_f	average spacing of small fractures (m)
SP_F	average spacing of large fractures (m)
t	time (s)
Δt	time step (s)
T	temperature (°C)
t_D	dimensionless time (defined in Table 2)
U_β	internal energy of phase β (J/kg)
U_s	internal energy of rock solids (J/kg)
V_n	volume of element n (m^3)
v_β	Darcy's velocity of phase β (m/s)
X_β^κ	mass fraction of component κ in phase β

Greek symbols

α_{Ff}	shape factor (m^{-2}) governing interflow between large fracture and small fracture
α_{FM}	shape factor (m^{-2}) governing interflow between large fracture and matrix
α_{fM}	shape factor (m^{-2}) governing interflow between small fracture and matrix
ϕ_f	effective porosity of a small fracture continuum
ϕ_F	effective porosity of a large fracture continuum
ϕ_M	effective porosity of a matrix continuum
γ	active fracture parameter
λ_{Ff}	F–M interporosity parameter (defined in Table 2)
λ_{FM}	F–f interporosity parameter (defined in Table 2)
λ_{fM}	f–M interporosity parameter (defined in Table 2)
λ_κ	radioactive decay constant of the chemical species κ (s^{-1})
μ	viscosity of fluid (Pa s)
ρ	density of fluid at in situ conditions (kg/m^3)
ρ_i	density of fluid at reference or initial conditions (kg/m^3)
ρ_β	density of phase β at in situ conditions (kg/m^3)
ρ_s	density of rock grains (kg/m^3)
ω_f	f storativity ratio (defined in Table 2)
ω_F	F storativity ratio (defined in Table 2)
ω_M	M storativity ratio (defined in Table 2)

Subscripts

e	effective
f	small fracture
F	large fracture
M	matrix
s	rock solid or surface ratio
th	thermal
β	index for fluid phase

Superscripts

E	energy
κ	index for mass components

Acknowledgements

The authors would like to thank G. Zhang, C. Doughty, and J. Liu for their review of the manuscript. Thanks are also due to K. E. Zellmer, J. Liu and L. Pan for their help in this work. This work was in part supported by the Director, Office of Civilian Radioactive Waste Management, U.S. Department of Energy, through Memorandum Purchase Order EA9013MC5X between Bechtel SAIC, LLC, and the Ernest Orlando Lawrence Berkeley National Laboratory (Berkeley Lab). The support is provided to Berkeley Lab through the U.S. Department of Energy Contract No. DE-AC03-76SF00098.

References

Abdassah, D., Ershaghis, I., 1986. Triple-porosity system for representing naturally fractured reservoirs. SPE Form. Eval. 1, 113–127.

Ahlers, C.F., Liu, H.H., 2000. Calibrated properties model. Report MDL-NBS-HS-000003. Berkeley, CA: Lawrence Berkeley Laboratory. Las Vegas, Nevada: CRWMS M&O.

Ahlers, C.F., Bandurraga, T.M., Bodvarsson, G.S., Chen, G., Finsterle, S., Wu, Y.S., 1995. Performance Analysis of the LBNL/USGS Three-dimensional Unsaturated Zone Site-scale Model, Yucca Mountain Project Milestone 3GLM105M. Lawrence Berkeley National Laboratory, Berkeley, CA.

Bai, M., Elsworth, D., Roegiers, J.C., 1993. Multiporosity/multipermeability approach to the simulation of naturally fractured reservoirs. Water Resour. Res. 29, 1621–1633.

Banddurraga, T.M., Bodvarsson, G.S., 1999. Calibrating hydrogeologic parameters for the 3-D site-scale unsaturated zone model of Yucca Mountain, Nevada. J. Contam. Hydrol. 38 (1–3), 25–46.

Barenblatt, G.I., Zheltov, I.P., Kochina, I.N., 1960. Basic concepts in the theory of seepage of homogeneous liquids in fissured rocks, PMM. Sov. Appl. Math. Mech. 24 (5), 852–864.

Bodvarsson, G.S., Liu, H.H., Ahlers, R., Wu, Y.S., Sonnethal, E., 2001. Parameterization and upscaling in modeling flow and transport at Yucca Mountain. In: Conceptual Models of Flow and Transport in the Fractured Vadose Zone. National Academy Press, Washington D.C., pp. 335–365.

Buesch, D.C., Spengler, R.W., Nelson, P.H., Vaniman, D.T., Chipera, S.J., Bish, D.L., 1995. Geometry of the vitric-veolitic transition in tuffs and the relation to fault Zones at Yucca Mountain, Nevada. International Union of Geodesy and Geophysics, XXI General Assembly, July 2–14, 1995.

Closemann, P.J., 1975. The aquifer model for fissured fractured reservoir. Soc. Pet. Eng. J., 385–398.

Doughty, C., 1999. Investigation of conceptual and numerical approaches for evaluating moisture, gas, chemical, and heat transport in fractured unsaturated rock. J. Contam. Hydrol. 38 (1–3), 69–106.

Earlougher Jr., R.C., 1977. Advances in well test analysis. SPE Monograph, vol. 5. SPE of AIME, Dallas.

Hevesi, J., Flint, L., 2000. Simulation of net infiltration for modern and potential future climate. Report ANL-NBS-GS-000008. Denver, Colorado: U.S. Geological Survey.

Kazemi, H., 1969. Pressure transient analysis of naturally fractured reservoirs with uniform fracture distribution. Soc. Pet. Eng. J., 451–462;
Pressure transient analysis of naturally fractured reservoirs with uniform fracture distribution. Trans. AIME, 246.

Kazemi, H., Dilman, J.R., Elsharkawy, A.E., 1992. Analytical and numerical solution of oil recovery from fractured reservoirs with empirical transfer functions. SPE Reservoir Engineering, 219–227.

Liu, H.H., Doughty, C., Bodvarsson, G.S., 1998. An active fracture model for unsaturated flow and transport in fractured rocks. Water Resour. Res. 34, 2633–2646.

Liu, H.H., Ahlers, C.F., Cushey, M.A., 2000. Analysis of Hydrologic Properties. Report ANL-NBS-HS-000002. Berkeley, CA: Lawrence Berkeley Laboratory, Las Vegas, Nevada: CRWMS M&O.

Liu, H.H., Bodvarsson, G.S., Finsterle, S., 2003. A note on unsaturated flow in two-dimensional fracture networks. Water Resour. Res. 36 (9), 15-1–15-9.

Liu, J.C., Bodvarsson, G.S., Wu, Y.S., 2003. Analysis of pressure behavior in fractured lithophysal reservoirs. J. Contam. Hydrol. 62–63, 189–211.

Liu, H.H., Haukwa, C.B., Ahlers, C.F., Bodvarsson, G.S., Flint, A.L., Guertal, W.B., 2003. Modeling flow and transport in unsaturated fractured rocks: An evaluation of the continuum approach. J. Contam. Hydrol. 62–63, 173–188.

McLaren, R.G., Forsyth, P.A., Sudicky, E.A., VanderKwaak, J.E., Schwarltz, F.W., Kessler, J.H., 2000. Flow and transport in fractured tuff at Yucca Mountain: numerical experiments on fast preferential flow mechanisms. J. Contam. Hydrol. 43, 211–238.

Montazer, P., Wilson, W.E., 1984. Conceptual hydrologic model of flow in the unsaturated zone, Yucca Mountain, Nevada. Water-Resources Investigations Report 84-4345. U.S. Geological Survey, Lakewood, CO.

Pollock, D.W., 1986. Simulation of fluid flow and energy transport processes associated with high-level radioactive waste disposal in unsaturated alluvium. Water Resour. Res. 22 (5), 765–775.

Pruess, K., 1983. GMINC—A mesh generator for flow simulations in fractured reservoirs. Report LBL-15227. Berkeley, CA: Lawrence Berkeley National Laboratory.

Pruess, K., 1991. TOUGH2—A general purpose numerical simulator for multiphase fluid and heat flow. Report LBL-29400, UC-251. Berkeley, CA: Lawrence Berkeley National Laboratory.

Pruess, K., Narasimhan, T.N., 1985. A practical method for modeling fluid and heat flow in fractured porous media. Soc. Pet. Eng. J. 25, 14–26.

Rulon, J., Bodvarsson, G.S., Montazer, P., 1986. Preliminary Numerical Simulations of Groundwater Flow in the Unsaturated Zone, Yucca Mountain, Nevada. LBL-20553. Lawrence Berkeley Laboratory, Berkeley, CA.

Snow, D.T., 1965. A parallel plate model of fractured permeable media, PhD dissertation. University of California, Berkeley, CA. 331 pp.

Sudicky, E.A., McLaren, R.G., 1992. User's guide for Fractran: an efficient simulators for two-dimensional, saturated groundwater flow and solute transport in porous or discretely-fractured porous formations. Groundwater Simulations Group, Institute for Groundwater Research, University of Waterloo, Waterloo, Ontario, Canada N2L 3G1.

Tsang, Y.W., Pruess, K., 1987. A study of thermally induced convection near a high-level nuclear waste repository in partially saturated fracture tuff. Water Resour. Res. 23 (10), 1958–1966.

van Genuchten, M.Th., 1980. A closed-form equation for predicting the hydraulic conductivity of unsaturated soils. Soil Sci. Soc. Am. J. 44 (5), 892–898.

Warren, J.E., Root, P.J., 1963. The behavior of naturally fractured reservoirs. Soc. Pet. Eng. J., 245–255; The behavior of naturally fractured reservoirs. Trans. AIME, 228.

Wittwer, C., Chen, G., Bodvarsson, G.S., Chornack, M., Flint, A., Flint, L., Kwicklis, E., Spengler, R., 1995. Preliminary Development of the LBL/USGS Three-Dimensional Site-Scale Model of Yucca Mountain, Nevada. LBL-37356. Lawrence Berkeley Laboratory, Berkeley, CA.

Wu, Y.S., 2000. On the effective continuum method for modeling multiphase flow, multicomponent transport and heat transfer in fractured rock. In: Faybishenko, B., Witherspoon, P.A., Benson, S.M. (Eds.), Dynamics of Fluids in Fractured Rocks, Concepts and Recent Advances. AGU Geophysical Monograph, vol. 122. American Geophysical Union, Washington, DC, pp. 299–312.

Wu, Y.S., Ge, J.L., 1983. The transient flow in naturally fractured reservoirs with three-porosity systems. Acta Mech. Sin. Theor. Appl. Mec. Beijing China 15 (1), 81–85.

Wu, Y.S., Pruess, K., 1988. A multiple-porosity method for simulation of naturally fractured petroleum reservoirs. SPE Reserv. Eng. 3, 327–336.

Wu, Y.S., Pruess, K., 2000. Numerical simulation of non-isothermal multiphase tracer transport in heterogeneous fractured porous media. Adv. Water Resour. 23, 699–723.

Wu, Y.S., Ahlers, C.F., Fraser, P., Simmons, A., Pruess, K., 1996. Software qualification of selected TOUGH2 modules. Report LBNL-39490. Lawrence Berkeley National Laboratory, Berkeley, CA.

Wu, Y.S., Ritcey, A.C., Ahlers, C.F., Hinds, J., Mishra, A.K., Haukwa, C., Liu, H.H., Sonnenthal, E.L., Bodvarsson, G.S., 1998. 3-D UZ site-scale model for abstraction in TSPA-VA, Yucca Mountain Project Level 4 Milestone Report SLX01LB3. Lawrence Berkeley National Laboratory, Berkeley, CA.

Wu, Y.S., Haukwa, C., Bodvarsson, G.S., 1999. A site-scale model for fluid and heat flow in the unsaturated zone of Yucca Mountain, Nevada. J. Contam. Hydrol. 38 (1–3), 185–215.

Wu, Y.S., Liu, J. Xu, T., Haukwa, C., Zhang, W., Liu, H.H., Ahlers, C.F., 2000. UZ flow models and submodels. Report MDL-NBS-HS-000006. Lawrence Berkeley National Laboratory, CRWMS M&O.

Wu, Y.S., Pan, L., Zhang, W., Bodvarsson, G.S., 2002. Characterization of flow and transport processes within the unsaturated zone of Yucca Mountain. J. Contam. Hydrol. 54, 215–247.